THE JOURNAL OF PHYSICAL CHEMISTRY C

pubs.acs.org/JPCC

Article

Ultrafast Charge-Transfer Exciton Dynamics in C_{60} Thin Films

Sebastian Emmerich,* Sebastian Hedwig, Benito Arnoldi, Johannes Stöckl, Florian Haag, Ralf Hemm, Mirko Cinchetti, Stefan Mathias, Benjamin Stadtmüller,* and Martin Aeschlimann

Cite This: J. Phys. Chem. C 2020, 124, 23579−23587

Read Online

ACCESS | Metrics & More | Article Recommendations | Supporting Information

ABSTRACT: The high flexibility of organic molecules offers great potential for designing the optical properties of optically active materials for the next generation of optoelectronic and photonic applications. However, despite successful implementations of molecular materials in today's display and photovoltaic technology, many fundamental aspects of the light-to-charge conversion in molecular materials have still to be uncovered. Here, we focus on the ultrafast dynamics of optically excited excitons in C_{60} thin films depending on the molecular coverage and the light polarization of the optical excitation. Using time- and momentum-resolved photoemission with femtosecond extreme ultraviolet (fs-XUV) radiation, we follow the exciton dynamics in the excited states while simultaneously monitoring the signatures of the excitonic charge character in the renormalization of the molecular valence band structure. Optical excitation with visible light results in the instantaneous formation of charge-transfer (CT) excitons, which transform stepwise into Frenkel-like excitons at lower energies. The number and energetic position of the CT and Frenkel-like excitons within this cascade process are independent of the molecular coverage and the light polarization of the optical excitation. In contrast, the depopulation times of the CT and Frenkel-like excitons depend on the molecular coverage, while the excitation efficiency of CT excitons is determined by the light polarization. Our comprehensive study reveals the crucial role of CT excitons for the excited-state dynamics of homomolecular fullerene materials and thin films.

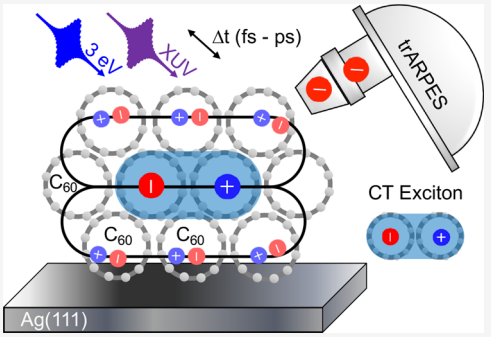

1. INTRODUCTION

The growing interest in molecular materials for application-oriented research as well as for fundamental studies is caused by their exceptional optical properties. Most importantly, the optical band gap of molecular materials can be actively controlled by tuning the molecular structure and composition using chemical synthesis.[1−3] This allows one to design and optimize their light absorption spectrum for photovoltaic applications. Despite this prospective of molecular materials for applications, many fundamental aspects of the light−matter interaction in molecular materials are still unsolved.

One of these challenges concerns the light-to-charge conversion process in molecular materials. Optical excitation of molecular thin films with visible light results in the formation of bound electron−hole pairs called excitons. In contrast to inorganic semiconductors, where excitons are only weakly bound and dissociate easily at room temperature, excitons in organic molecules are considerably more stable, with binding energies up to 1 eV.[4] These excitons can exhibit different degrees of localization and different spatial charge distributions depending on their excited-state energy.[5−7] For optical excitation energies in the range of the fundamental band gap, the electron−hole pairs are typically located on a single molecular site; that is, they can be described as Frenkel-like excitons. For larger photon energies, the created excitons can be either highly excited Frenkel excitons or charge-transfer (CT) excitons, with electrons and holes being separated on neighboring molecular sites. The charge-transfer character of these excitons together with the corresponding delocalization of the charges of the electron hole-pair lay the foundation for exciton dissociation processes and the formation of free charge carriers in homomolecular materials at room temperature.[5,6]

So far, the formation and decay processes of CT excitons have been investigated most frequently at heteromolecular interfaces between donor and acceptor molecules[8−13] as well as in organic polymer films where these CT excitons are often referred to as interchain excitons.[14,15]

In contrast, only a few studies focused on the role of CT excitons in homomolecular structures and thin films of small aromatic molecules, despite their crucial role for the exciton decay process.[6,7,16,17] This is mainly because the spectroscopic signatures of Frenkel-like and CT-like excitons are extremely difficult to distinguish experimentally.

In this context, we recently uncovered a new and clear spectroscopic signature of CT excitons in molecular solids by

Received: September 2, 2020
Revised: September 25, 2020
Published: October 15, 2020

https://dx.doi.org/10.1021/acs.jpcc.0c08011
J. Phys. Chem. C 2020, 124, 23579−23587

studying the exciton dynamics of C_{60} thin films.[17] Using time-resolved photoemission experiments with femtosecond radiation in the extreme ultraviolet (XUV, 22.2 eV) spectral range,[18−21] we were able to simultaneously monitor the exciton dynamics in the excited states and the transient band structure dynamics of the (occupied) molecular valence band structure of the molecules surrounding the optically generated exciton. We observed the formation and the subsequent population decay cascade of optically generated excitons in the excited states. The exciton dynamics of the two highest excited states coincide with the time scales of the transient spectral broadening of all molecular features in the valence band. This inhomogeneous spectral broadening of all valence states was identified as the spectroscopic signature of CT excitons in molecular films. It is caused by the spatial extension of the charge distribution and the corresponding strength of the dipole or multipole moment of the excitons. These local dipole moments associated with CT excitons severely alter the local energy level alignment of the molecules surrounding the exciton. Thereby, the sign and magnitude of the energy shifts of the valence states of the individual molecules within the film critically depend on their distance and relative position with respect to the charge-transfer exciton. This leads to a spatially varying transient energy level alignment of the C_{60} film on the nanometer scale that causes the inhomogeneous broadening of the molecular valence band states in the spatially averaging photoemission experiments.

Taking advantage of this signature of CT excitons, we revisited the exciton dynamics of a C_{60} thin film after excitation with 3.2 eV photons. This photon energy is, in general, large enough to optically excite a manifold of highly excited Frenkel and CT excitons.[5−7] We were able to show that resonant optical excitation with 3.2 eV photons instantaneously results in the formation of an excitonic state. Crucially, the population dynamics of this excitonic state coincide almost perfectly with the temporal evolution of the initial inhomogeneous broadening of all valence states of the C_{60} film. This provides clear evidence that the majority of optically excited excitons are charge-transfer excitons with the hole located in the highest occupied molecular orbital (HOMO) of one molecular site and the electron in the second lowest unoccupied molecular orbital (LUMO+1) of a neighboring molecular site. These optically excited CT excitons directly decay into lower lying CT excitons with less prominent charge-transfer character before transforming into a Frenkel-like exciton with electron and hole on identical molecular sites.

In this work, we extend our recent study of the dynamics of CT and Frenkel excitons in thin C_{60} films on Ag(111). Using the same experimental approach as introduced in ref 17, we explore the ultrafast dynamics of CT and Frenkel excitons in thin C_{60} films for various film thicknesses and light polarizations. Finally, we demonstrate that the transient broadening can be observed in the complete valence band structure of the C_{60} thin films throughout the entire Brillouin zone, thereby directly probing the potential influence of dispersion and cross section effects. We find an increase of the CT exciton stability with increasing C_{60} coverage and the independence of the exciton decay dynamics on the light polarization. In this way, our results lead to a refined understanding of the accessibility of the CT exciton dynamics via the many body response and the band structure renormalization of the surrounding molecules. This opens a new opportunity for tracing CT exciton in molecular and other low dimensional semiconductor (hetero) structures on ultrafast time scales.

2. METHODS

2.1. Sample Preparation. All sample preparation steps have been performed under ultrahigh vacuum (UHV) conditions. The Ag(111) single crystal substrate has been cleaned by several cycles of Ar^+-sputtering and subsequent sample annealing at 730 K. The cleanness of the sample surface has been confirmed by sharp diffraction maxima in low energy electron diffraction (LEED) experiments and by monitoring the existence and line width of the Shockley surface state at the $\bar{\Gamma}$-point of the surface Brillouin zone. The C_{60} molecules have been evaporated onto the clean Ag(111) surface at a pressure $<10^{-9}$ mbar using a Knudsen-type evaporation source. The molecular flux used during the evaporation process was calibrated using a quartz crystal oscillator gauge. The gauge has been calibrated prior to the experiment by monitoring the peak positions of the C_{60} valence band structure as well as the work function of the C_{60} films and comparing both quantities to values from the literature.[22,23] The crystalline structure of the C_{60} thin film has been confirmed by LEED.[24]

2.2. Time- and Angle-Resolved Photoemission Spectroscopy. For the time (and angle)-resolved photoemission experiments, a hemispherical electron spectrometer (SPECS Phoibos 150), a high-precision six-axis manipulator, and a femtosecond extreme ultraviolet (fs-XUV), 22.2 eV light source have been combined.

The fs-XUV radiation is obtained by high harmonic generation (HHG).[25] The detailed description of our setup can be found in refs 26 and 27. In short, our fs-XUV light source is based on a regenerative titanium-sapphire chirped-pulse amplifier with sub-50 fs pulse duration, 10 kHz repetition rate, and a pulse energy of 1 mJ at a wavelength of 780 nm. Typically, 90% of the beam intensity is used for the HHG process. First, the radiation of the laser amplifier systems is frequency-doubled in a β-barium borate (BBO) crystal and subsequently focused into a hollow waveguide, filled with 30 Torr of Kr, where the HHG process takes place. For our experimental conditions, the high harmonic spectrum exhibits a strong emission line at 22.2 eV (seventh harmonic of the HHG spectrum), which is separated by 6.4 eV from the neighboring emission lines (fifth and ninth harmonics of the HHG spectrum) and has a spectral bandwidth (fwhm) of ∼150 meV. The HHG radiation is linearly polarized and the orientation of the light polarization (p- or s-polarization with respect to the sample surface) can be adjusted by controlling the light polarization of laser radiation driving the HHG. After the fs-XUV radiation is guided through a set of transmissive Al and Sn filters with thicknesses of $d_{Al} = 0.2$ μm and $d_{Sn} = 0.1$ μm, respectively, it is focused onto the sample surface using a toroidal mirror.

The remaining 10% of the beam intensity of the titanium sapphire amplifier (∼0.1 mJ) is available for the optical excitation of the C_{60} films. This part of the beam is frequency-doubled in a second BBO crystal (resulting in a photon energy of 3.2 eV with a spectral bandwidth of 0.04 eV) and is focused on the sample surface. The polarization of the pump pulse is adjusted with a combination of a linear polarizer and a half-wave plate. The delay between the optical pump and the fs-XUV probe pulse is controlled by a delay stage operating with 1 μm longitudinal resolution.

Prior to each experiment, the spatial and temporal overlap of the pump and the probe pulse on the sample surface was carefully adjusted and checked regularly during the series of measurements. For each sample, we also characterized the

https://dx.doi.org/10.1021/acs.jpcc.0c08011
J. Phys. Chem. C 2020, 124, 23579−23587

influence of pump- or probe-induced space charge effects on the temporal and spectral shape of our time-resolved photoemission data. For all experiments shown throughout this Article, we limited the power of the pump and probe beam to fluences that do not cause a time-dependent energy shift or a time-dependent line width broadening larger than our experimental uncertainty and that follow the typical time scale of space charge effects.[28] Furthermore, the molecular thin films were checked regularly for radiation-induced degradation or dimerization.[29]

In our experiments, we selected analyzer operating parameters, which allowed us to record an energy versus momentum range of 6.4 eV versus 0.8 $Å^{-1}$ in a single acquisition. Additional momentum-resolved photoemission data were obtained by turning the azimuthal and polar angle of our six-axis manipulator system. The latter was used in our time- and angle-resolved photoemission experiment to align the $\bar{\Gamma}\bar{M}$-direction of the main structural domain of the C_{60} film parallel to the entrance slit of the hemispherical analyzer. The band structure along the $\bar{\Gamma}\bar{M}$-direction of higher Brillouin zones is accessed experimentally by rotating the polar angle of our sample manipulator. Prior to each experiment, the orientations of the different structural domains of the C_{60} thin films were determined by low energy electron diffraction.

3. RESULTS AND DISCUSSION

3.1. Coverage-Dependent Exciton Dynamics.

3.1.1. Population Dynamics. We start our investigation with the coverage-dependent exciton dynamics of C_{60} thin films on an Ag(111) crystal for molecular coverages between 2 and 20 ML. We focus particularly on the transient band structure dynamics of the valence band structure and its correlation to the population dynamics of the excited states in the so-called single-particle excitation regime. To this end, we only apply fluences between 10 and 100 $\mu J\ cm^{-2}$. These fluences lead to exciton dynamics in the linear regime where the time scales of the exciton dynamics do not depend on the applied fluence and are hence sufficiently low to avoid nonlinear effects and the formation of trions or biexcitions.[17]

For all coverages, we find a qualitatively identical excited-state dynamics after optical excitation, with quantitative differences depending on film thickness and light polarization of the exciting light pulses. The exciton dynamics is shown exemplarily in the 2D plot of the excited states of a C_{60} film ($\Theta_{C60} = 15$ ML) and is summarized in the energy level diagram in Figure 1. The latter is based on the findings of previous investigations dedicated to the excited-state energy level alignment of C_{60} thin films.[7,17,30−35]

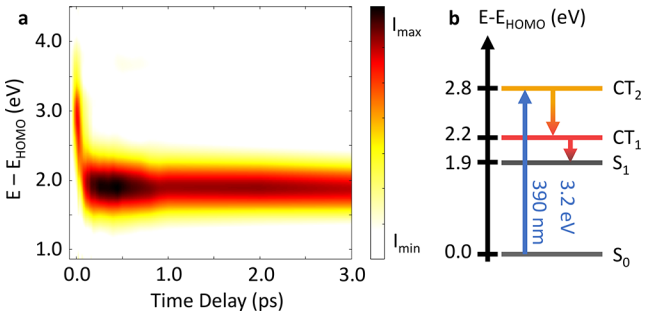

Figure 1. (a) 2D plot of the time-resolved photoemission data of the excited-state energy range of a C_{60} film ($\Theta_{C60} = 15$ ML) after optical excitation with femtosecond-light pulses ($h\nu = 3.2$ eV). (b) Energy level diagram of the excitonic states of the C_{60} thin film.

Optical excitation with 3.2 eV photons leads to the instantaneous formation of excitons with pronounced charge-transfer character at $E - E_{HOMO} \approx 2.8$ eV, labeled CT_2. These CT_2 excitons are resonantly excited from the HOMO level despite the energy mismatch between the intrinsic excited-state energy of the CT_2 excitons ($E_{CT2} - E_{HOMO} = 2.8$ eV) and the photon energy of the optical excitation. This is possible due to the extremely large line width of the HOMO and the CT_2 exciton level in conjunction with the spectral bandwidth of the ultrashort pump pulses. The charge-transfer character of these excitons has recently been confirmed experimentally by identifying the existence of characteristic dipole or multipole moments for the CT_2 excitons that are associated with delocalized charge-transfer excitons.[6,7,17] The CT_2 excitons decay almost instantaneously ($\tau_{CT2} < 100$ fs) and repopulate another excitonic level with partial CT character at lower energies (referred to as CT_1 excitons). The electrostatic dipole or multipole moment associated with the CT_1 exciton is significantly smaller as compared to the CT_2 exciton.[7,17] It is therefore speculated that the CT_1 excitons consist of both CT and Frenkel exciton character.[7] Finally, the population of the CT_1 level decays further into a Frenkel-like excitonic state (referred to as S_1-excitons) where the excitons are trapped for nanoseconds.[31,32]

The population dynamics of the excitons are quantified by analyzing the spectral intensity of the time-resolved photoemission data of the excited states using the same fitting procedure as developed in ref 17. Background-corrected photoemission spectra at selected time delays as well as more details on the data analysis procedure are shown in the Supporting Information. The resulting transient populations of the CT_2-, CT_1-, and S_1-excitons are shown exemplarily in Figure 2a,b for molecular coverages of $\Theta_{C60} = 2$ ML and $\Theta_{C60} = 15$ ML. The data points including the experimental uncertainty are shown in orange, red, and grey dots for the CT_2-, CT_1-, and S_1-excitonic levels. The corresponding dynamics of the CT_2 and the CT_1 exciton are fitted by two exponential functions to model its population $\bar{\tau}$ and depopulation τ time. The best fitting results are included in Figure 2a,b as solid lines of color identical to that of the data points. For both coverages, we find extremely fast depopulation time constants of the CT_2 exciton of $\tau_{CT2}(2\ ML) = 40 \pm 10$ fs and $\tau_{CT2}(15\ ML) = 38 \pm 10$ fs for the 2 ML film and 15 ML films, respectively. For each coverage, these depopulation time constants τ_{CT2} are identical to the population time constants $\bar{\tau}_{CT1}$ of the energetically lower CT_1 exciton, suggesting a direct decay from the CT_2 to the CT_1 exciton. In contrast to the CT_2 exciton, the depopulation times of the CT_1 exciton are significantly different for both coverages and reveal values of $\tau_{CT1}(2\ ML) = 310 \pm 70$ fs and $\tau_{CT1}(15\ ML) = 1.5 \pm 0.3$ ps; that is, the depopulation time τ_{CT1} increases with increasing coverage. A coverage-dependent lifetime of highly excited excitons such as the CT_1 exciton has already been reported previously and is attributed to the increasing distance between the excited excitons and the substrate electrons for larger film thicknesses. The latter limits the number of interaction channels and scattering processes between the excitons and the surface electrons, for instance, by charge-transfer processes, which reduces the depopulation time of excited excitons in molecular films with increasing film thickness.[34]

https://dx.doi.org/10.1021/acs.jpcc.0c08011
J. Phys. Chem. C 2020, 124, 23579−23587

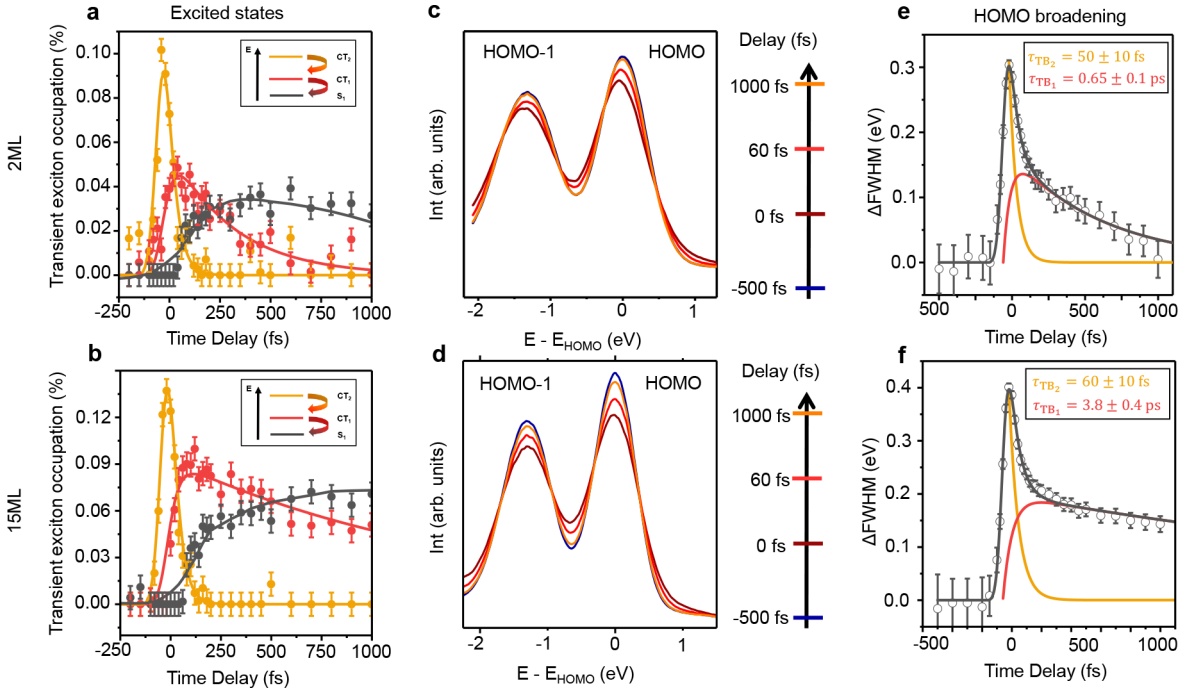

Figure 2. (a,b) Femtosecond transient population dynamics of the excitonic levels of the 2 ML film (a) and the 15 ML film (b), showing the extracted dynamics of populations for CT_2, CT_1, and S_1. The rise and decay times of CT_2 and CT_1 are determined by exponential fitting functions (for more details, see the Supporting Information), which are shown in color identical to that of the corresponding data points. In contrast, the solid line of the S_1 exciton is only a guide to the eye. (c,d) Background-corrected photoemission spectra for selected pump−probe time delays, showing the transient broadening of the HOMO levels of the 2 ML film (c) and the 15 ML film (d). (e,f) Transient broadening of the HOMO levels, extracted by a spectral analysis from the energy distribution curves shown in (c) and (d) of the 2 ML film (e) and the 15 ML film (f). Following the dynamics of the excited states in the population dynamics (a,b), the fast decay constant τ_{TB2} is independent of the C_{60} coverage, while the slow decay constant τ_{TB1} strongly increases with the film thickness. The rise of the red fitting curve around $\Delta t = 0$ describing the slow decay constant is based on the modeling of the refilling of CT_1, with $\tau_{rise,TB2} = \tau_{TB1}$.

Similarly, the depopulation time of the Frenkel exciton τ_{S1} also increases with increasing coverage, in agreement with recent studies of the exciton dynamics of molecular materials.[30,32,36]

3.1.2. Transient Evolution of Molecular Valence Band Structure. Next, we turn to the transient band structure renormalization of the molecular ensemble, which reflects the charge character of the optically excited excitons. For CT excitons, the separation of electron and hole results in a first approximation in a significant electric moment that will affect the energy levels of the polarizable surrounding molecular film[17] to result in a shift of the energy levels of the individual molecules in the vicinity of the CT exciton. On average, these individual shifts add up to an inhomogeneous line width broadening of the molecular energy levels in the spatial region of the probe pulse on the sample surface. These transient line width dynamics can be extracted from our data by monitoring the transient renormalization of the valence band structure. Background-corrected photoemission spectra in the energy region of the HOMO and the HOMO−1 states at selected time delays are shown for both molecular coverages in Figure 2c,d. In both cases, we observe an instantaneous increase of the line width of both molecular states upon optical excitation, which reduces again on the picosecond time scale. This transient broadening is induced by the formation of CT excitons in both C_{60} films upon optical excitation, independent of the molecular coverage. To quantify the dynamics of the CT excitons in the C_{60} film, we analyze the transient broadening of the molecular valence band structure using the fitting procedure established in ref 17. More details can be found in the Supporting Information. The extracted transient broadening traces for the HOMO level for both molecular films are shown in Figure 2e,f. For both cases, the best fitting result is obtained by using a double-exponential decay function with decay constants that are comparable with the depopulation times τ_{CT2} and τ_{CT1} of the excited states of the corresponding molecular film. In particular, we find $\tau_{TB2}(2\,ML) = 50 \pm 10\,fs$, $\tau_{TB1}(2\,ML) = 650 \pm 100\,fs$, $\tau_{TB2}(15\,ML) = 60 \pm 10\,fs$, and $\tau_{TB1}(15\,ML) = 3.8 \pm 0.4\,ps$. Most importantly, these time scales are significantly shorter than the decay constant of the S_1-exciton, which is on the order of nanoseconds. Consequently, the transient broadening is not affected by the population dynamics of the S_1-exciton. This allows us to confirm that only the excitonic levels CT_2 and CT_1 reveal a significant CT exciton character for both coverages, while, in both cases, the S_1-exciton exhibits exclusive Frenkel exciton-like character.

A qualitatively similar transient band structure dynamics can be detected for all molecular coverages between 2 and 20 ML. This is clearly visible in Figure 3a, which shows the transient broadening of the HOMO level obtained for five molecular films with different coverage. The extracted decay constant τ_{TB1}, corresponding to the CT_1 decay (τ_{CT1}), is shown in Figure 3b. The decay time of the energetically lowest CT exciton (CT_1) into the Frenkel exciton-like state S_1 increases continuously with increasing coverage before saturating at around 15−20 ML. The asymptotic values for the exciton decay hence reflect the intrinsic dynamics of CT excitons of the fullerene thin film.

https://dx.doi.org/10.1021/acs.jpcc.0c08011
J. Phys. Chem. C 2020, 124, 23579−23587

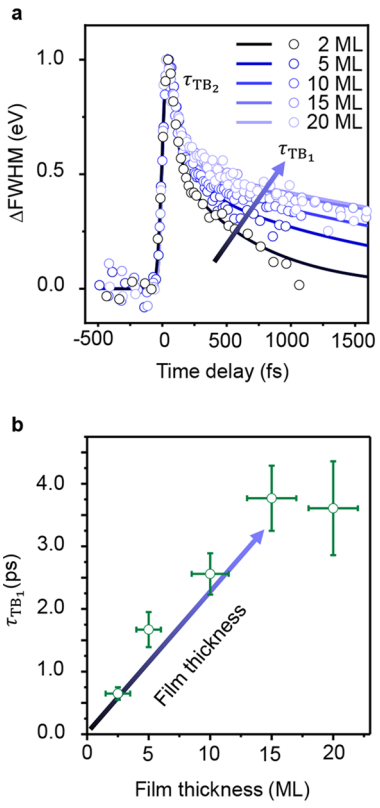

Figure 3. (a) The transient line width broadening of the valence states, extracted for several film thicknesses. They show a constant fast decay time τ_{TB2} and an increase of the slow decay time τ_{TB1} with increasing film thickness. (b) Correlation between the slow decay time τ_{TB1} and the C_{60} coverage. We find a monotonic increase of τ_{TB2}, as observed in (a), and a potential saturation for coverages above 15 ML.

In this regard, our investigation of the coverage-dependent exciton dynamics in C_{60} thin films allows us to draw the following conclusions:

(1) The double exponential decay dynamics of the transient broadening of all valence band states proofs that CT_2 and CT_1 are excitons with predominant charge-transfer character, while the S_1-exciton is of Frenkel-like character.

(2) The depopulation time τ_{CT1} of the CT_1 exciton increases with increasing molecular coverage.

Our findings hence do not only reflect the coverage-dependent exciton dynamics of fullerene thin films[30−32,34,36] and other molecular complexes[40] on various substrates. They also shine new light onto the coverage-dependent charge distribution of the optically excited excitons and their coverage-dependent relaxation processes back to the ground state.

Note that minor quantitative differences between our findings and the literature can be attributed to the significantly larger probe photon energy used in our experiment as compared to typical time-resolved photoemission studies of the exciton dynamics in molecular materials. This large photon energy of $h\nu$ = 22.2 eV results in an extremely high surface sensitivity of our experiment, which is typically not the case for low energy two-photon photoemission studies using laser light sources in the visible to ultraviolet range.[33,35]

3.2. Light Polarization-Dependent Exciton Dynamics.

Next, we characterize the influence of the polarization of the light on the creation and relaxation dynamics of excitons in the C_{60} films. The crystalline order of the C_{60} solid could potentially result in a finite crystal anisotropy despite the high symmetry of the C_{60} molecules themselves.

For the sake of completeness, we investigated four possible combinations of probe and pump light polarization. In our following abbreviations, the polarization of the probe will be named first, followed by the pump polarization; that is, ps refers to an experiment with a p-polarized probe and an s-polarized pump beam. In our experimental geometry with an incidence angle of 45° for the pump and probe radiation in normal emission geometry (see Figure 4a), p-polarized light exhibits an in-plane as well as an out-of-plane component of the electric field vector with respect to the surface plane. In contrast, the electric field vector of s-polarized light is located completely in the sample surface plane. To quantify the light polarization-dependent effects, we recorded the excited-state dynamics and the transient evolution of the valence states of a C_{60} thin film for each of these four combinations. As an exemplary case, we have selected a C_{60} film with a coverage of $\Theta_{C60} = 5 \pm 2$ ML. We find that the polarization of the probe beam mainly influences the overall photoemission yield of our experiment; that is, the photoemission cross section of the C_{60} film is significantly larger for p-polarized light as compared to s-polarized light.[38,39] We therefore normalized all photoemission spectra to the integrated intensity of the HOMO feature prior to the optical excitation to uncover spectral changes of the time-resolved photoemission spectra obtained either with p- or with s-polarized fs-XUV radiation.

Next, we turn to the light polarization of the pump pulse, which has a significant influence on the efficiency of the optically generated CT_2 excitons. Using a photon energy of 3.2 eV, we observe an optically generated population of the CT_2 exciton of $P_{CT2,p\text{-}pol}(0\text{ fs}) = (3.8 \pm 0.4) \times 10^{-3}$ for p-polarized light at an applied laser fluence of $F_p = 50 \pm 10\ \mu J\ cm^{-2}$. The exciton population at time zero $P_{CT2,p\text{-}pol}(0\text{ fs})$ is quantified by the integrated photoemission intensity of the CT_2 feature in the excited-state energy range (which was normalized beforehand to the integrated intensity of the HOMO prior to the optical excitation). For s-polarized light, a significantly larger applied laser fluence of $F_s = 70 \pm 10\ \mu J\ cm^{-2}$ is required to obtain a comparable exciton population of P_{CT2} (0 fs) = (4.0 ± 0.4) × 10^{-3}. The similar exciton population for these significantly different pump fluencies is also confirmed by the almost identical transient line width broadening of $\Delta fwhm_{p-pol}(0\text{ fs}) = 0.37 \pm 0.03$ eV and $\Delta fwhm_{s-pol}(0\text{ fs}) = 0.35 \pm 0.03$ eV for optical excitation with p- and s-polarized light. On the basis of these findings, we can estimate that the exciton excitation efficiency of s-polarized light is only 69 ± 15% of the exciton excitation efficiency of p-polarized light; that is, the exciton generation efficiency is reduced by 31 ± 15% when changing from p-polarized to s-polarized pump pulses. This difference in absorption can be attributed to the different reflection and transmission of p- and s-polarized light at the vacuum/C_{60} interface. The latter can be estimated by the Fresnel equations. Using the experimentally determined index of refraction $n(\hbar\omega) = n_r(\hbar\omega) + in_i(\hbar\omega)$ of a C_{60} solid film[41] (n_r(3.2 eV) = 2.5 ± 0.1 and n_i(3.2 eV) = 1.25 ± 0.20), we find that the absorption of s-polarized light is 27 ± 9% smaller as compared to that of p-polarized light for the employed pump photon energy.

On the basis of these findings, we can conclude that the polarization of the pump pulse only alters the number of optically excited excitons, but not the energetic position and the charge character of the optically excited excitons. Therefore, we

https://dx.doi.org/10.1021/acs.jpcc.0c08011
J. Phys. Chem. C 2020, 124, 23579−23587

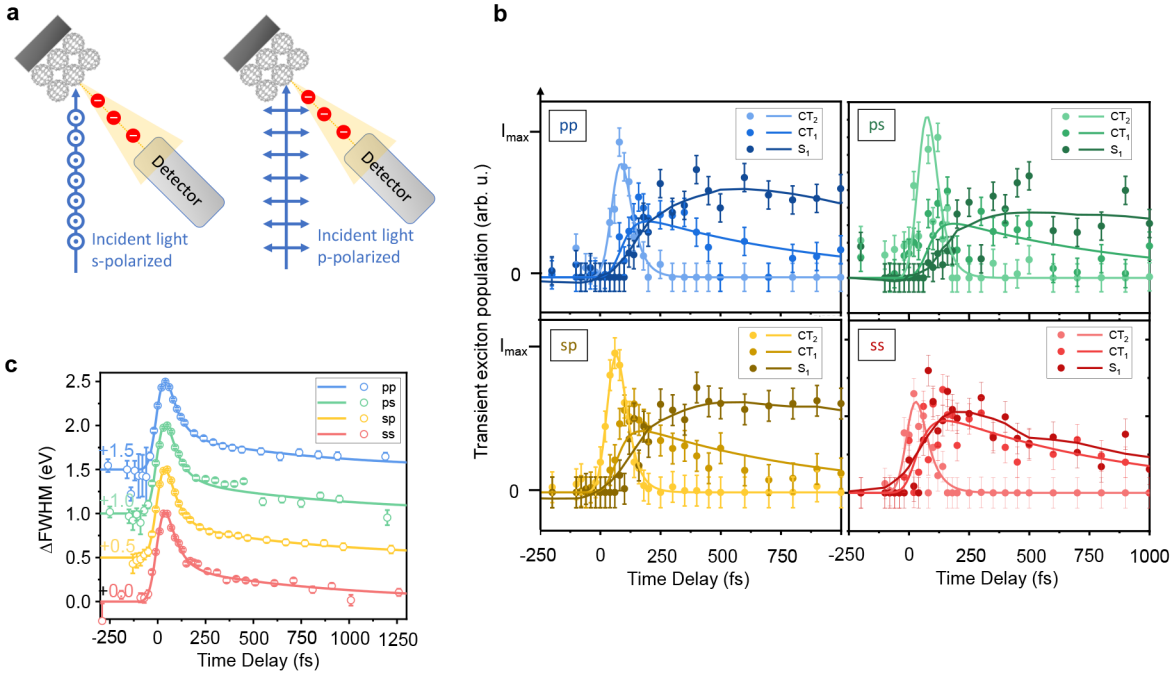

Figure 4. (a) Experimental geometry of the tr-photoemission study for different light polarizations. For s-polarized light (case left), the electric field relative to the sample is completely in-plane. For p-polarized light (case right), the electric field consists of a mixture of in-plane and out-of-plane components. (b) Optically induced population dynamics for the different combinations of pump and probe light polarization. The color of the CT_2 exciton dynamics reflects the color of the transient broadening in (c). The solid lines of the CT_2 and CT_1 exciton are exponential fitting functions (for more details, see the Supporting Information), while that of the S_1 exciton is a guide to the eye. (c) Transient broadening of the HOMO level for different combinations of probe and pump light polarization. The plots have been vertically shifted by 0.5 eV with respect to each other for better visibility. Similar to the invariance of the population dynamics, also the transient broadening dynamics are not affected by the pump and probe light polarization.

do not expect any influence of the light polarization of the pump pulse on the optically induced exciton dynamics.[17] The same is true for the light polarization of the probe pulse, which mainly affects the photoemission yield of the molecular valence bands. To verify this expectation, we extracted the population dynamics of the CT_2, CT_1, and S_1 excitons for all four combinations of light polarization using the same fitting routine as discussed above. The transient populations of these states are shown in Figure 4b. Interestingly, the maximum population of the CT_1 excitonic state seems to be lower as compared to that of the S_1 excitons for all combinations of light polarizations of the pump and the probe beam. This is clearly different as compared to the transient exciton populations of the 2 and 15 ML C_{60} films shown in Figure 2 where the maximum number of excitons decreases stepwise from CT_2 to S_1. So far, the reason for this discrepancy is unclear. However, we propose that the transient population of the CT_1 excitonic state is underestimated in Figure 4, possibly due to the limited signal-to-noise ratio of the corresponding data sets.

The population and depopulation time constants $\bar{\tau}$ and τ are obtained individually for each state using exponential functions. The best fitting results are included in Figure 4b as solid lines. For all four cases, the optical excitation results in an instantaneous formation of the CT_2 excitons. Subsequently, they transform extremely fast into the CT_1 excitons with $\tau_{CT2}(5\,ML) = \bar{\tau}_{CT1}(5\,ML) = 45 \pm 10$ fs. The decay time of the CT_1 state is $\tau_{CT1}(5\,ML) = 0.8 \pm 0.3$ ps, which is consistent with our coverage-dependent study of the exciton dynamics of C_{60} thin films. Note that these population and depopulation decay constants are identical for all four experiments within the experimental uncertainty. This points to polarization-independent population dynamics of the excitons in C_{60}.

A similar behavior can be observed for the transient line width broadening of the molecular valence states. In all four cases, the optical excitation instantaneously results in a transient line width broadening, which is quantified using a double-exponential decay fitting model as described in section 3.1.2. The evolution of the transient broadening Δfwhm of the HOMO level is shown for all four combinations of polarization in Figure 4c, revealing a double-exponential decay with identical decay constants of $\tau_{TB2} = 60 \pm 10$ fs and $\tau_{TB1} = 0.8 \pm 0.2$ fs.

Therefore, we can conclude that neither the spatial charge distribution nor the time scales of the excited excitons depend on the polarization of the exciting light pulses. This points to a highly isotropic behavior of the excitons in the thin films of the highly symmetric fullerene complexes. Moreover, it is important to mention that the transient line width broadening is also independent of the polarization of the probe radiation. This shows that the dipole or multipole moment of the CT-like exciton equally effects the energy level alignment of all valence states of neighboring molecules, independent of the orbital character of the valence states.

Interestingly, the light polarization-independent depopulation dynamics of the CT excitons allow us to further investigate the transient line width broadening of the valence states throughout the surface Brillouin zone of the C_{60} crystal structure with fixed light polarization of the pump and probe radiation. This becomes possible by choosing s-polarized pump and probe pulses for which the light polarization vector is aligned along the rotation axis of the sample in our time- and angle-resolved

https://dx.doi.org/10.1021/acs.jpcc.0c08011
J. Phys. Chem. C 2020, 124, 23579−23587

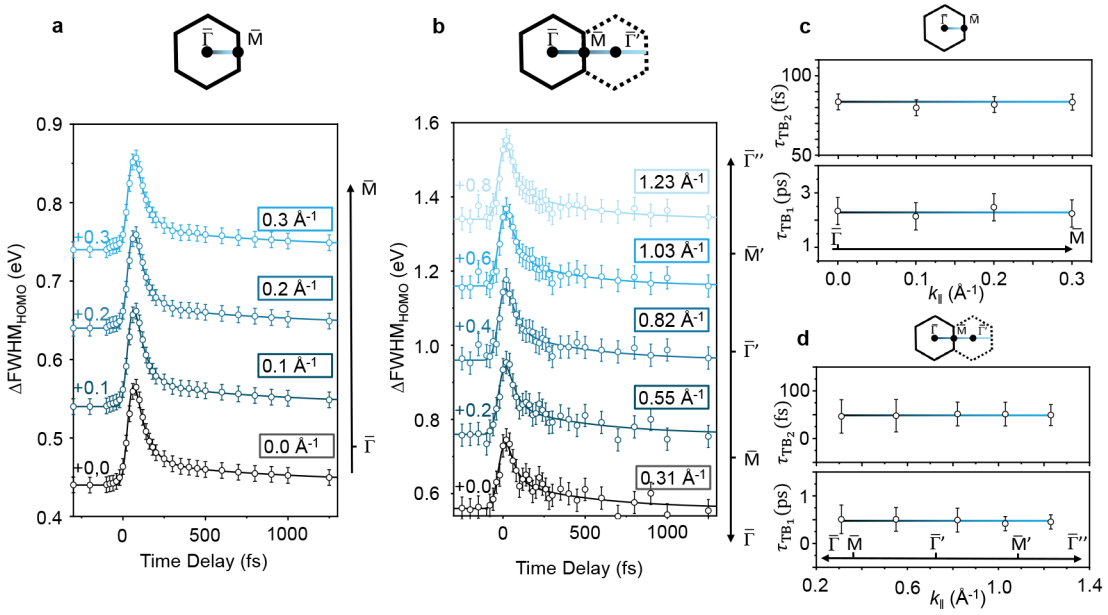

Figure 5. (a) Direct comparison of the transient line width broadening of the HOMO width for different momenta within the first Brillouin zone along the $\bar{\Gamma}\bar{M}$-direction (see sketch of Brillouin zone above). Each curve has been shifted vertically by 0.1 eV for better visibility. (b) Direct comparison of the transient HOMO width for different momenta in the $\bar{\Gamma}\bar{M}$-direction to the $\bar{M}$ point and beyond (see sketch above graph for orientation). The plots have been shifted by 0.2 eV vertically for better visibility. (c) Extracted decay times τ_{TB2} and τ_{TB1} for the transient HOMO width shown in (a). There is no change within error bars. (d) Extracted decay times τ_{TB2} and τ_{TB1} for the transient HOMO width shown in (b). There is no change within error bars. Note that the measurements for (a,c) and (b,d) were conducted on different sample preparations. Thus, the qualitative change of decay times between both measurements has its origin in different C_{60} coverages between the two C_{60} films as has been discussed previously.

photoemission experiment (as shown in Figure 4a). Taking advantage of this opportunity, we recorded time- and momentum-resolved photoemission data within the first surface Brillouin zone along the $\bar{\Gamma}\bar{M}$-direction of the C_{60} crystal structure. At room temperature, C_{60} forms a long-range ordered $(2\sqrt{3} \times 2\sqrt{3})30^{\circ}$ superstructure with two additional structural domains rotated by $\pm 15^{\circ}$.[24] These rotational domains exhibit identical electronic properties as the main structural domain with sinusoidal bands dispersing around the $\bar{\Gamma}$-points of the surface Brillouin zones. This high isotropy of the system still allows us to study the momentum-dependent transient broadening phenomena throughout the surface Brillouin zone of C_{60} despite the existence of three structurally inequivalent domains. The corresponding surface Brillouin zone of the central C_{60} domain is shown in Figure 5a, and the $\bar{\Gamma}\bar{M}$-direction is marked by a blue line. Time-resolved photoemission data sets were recorded in steps of 0.1 Å^{-1}, and the transient line shape of the entire valence band structure was analyzed using the same fitting model as discussed before. For the C_{60} crystal, the $\bar{M}$-point is reached at $k_{\parallel,\bar{M}} = 0.36$ Å^{-1}, with the $\bar{K}$-point at $k_{\parallel,\bar{K}} = 0.42$ Å^{-1}.[37]

The transient line width broadening of the HOMO level is shown in Figure 5a. For all points in the surface Brillouin zone, we observe an identical temporal evolution of the HOMO line width, similar to our findings discussed above. The HOMO line width increases instantaneously upon optical excitation, followed by a double-exponential decay. The decay constants of the double-exponential decay are $\tau_{TB2} = 82 \pm 10$ fs for the first decay step and $\tau_{TB1} = 2.3 \pm 0.5$ ps for the second one. Interestingly, the magnitude of the transient broadening, that is, the maximum transient line width broadening at $\Delta t = 0$ fs, Δfwhm(0 fs), is also identical for all momenta along the $\bar{\Gamma}\bar{M}$ -direction.

For a second C_{60} sample with slightly lower C_{60} coverage, we repeated the same experiment in a larger range of momenta covering also the second and third surface Brillouin zones of the C_{60} crystal. The transient line width broadening traces of the HOMO are shown in Figure 5b. All traces exhibit an identical shape, that is, an instantaneous rise with an identical maximal line width broadening Δfwhm(0 fs), followed by a double-exponential decay with identical decay constants of $\tau_{TB2} = 50 \pm 25$ fs and $\tau_{TB1} = 0.50 \pm 0.25$ ps.

The momentum-dependent decay times of the transient line width broadening of the C_{60} HOMO are summarized in Figure 5c,d. The different transient broadening times τ_{TB1} in the first and higher Brillouin zones in Figure 5c and d are due to the different C_{60} coverages used in the corresponding experiments. The time constants in Figure 5c and d clearly show that the transient line width broadening occurs simultaneously throughout the entire valence band structure with an equal amplitude Δfwhm(0 fs). The transient broadening itself thus only depends on the film thickness (as discussed earlier) and the strength of the optical excitation.[17] These observations are fully in line with our proposed model for the transient broadening: The optically excited CT excitons create a transient electrostatic (Stark-like) field that results in a transient polarization of the surrounding molecular material. In turn, this transient change in the dielectric screening results in a transient energy shift of the molecular valence states of the organic molecules surrounding the CT exciton. Crucially, the magnitude and sign of the transient band structure renormalization only depend on the relative position of the CT exciton and the probed molecule, and not on the specific binding energy or momentum of the molecular state. In this regard, our experiments are fully supported by our proposed

https://dx.doi.org/10.1021/acs.jpcc.0c08011
J. Phys. Chem. C 2020, 124, 23579−23587

model, predicting an equal shift of all molecular states, independent of their momentum.

4. CONCLUSION

In this work, we investigated the dynamics of CT and Frenkel excitons in thin C_{60} films on Ag(111), depending on the molecular coverage as well as on the light polarization of the optical excitation. Using time- and momentum-resolved photoemission with fs-XUV radiation, we followed the population dynamics of the excitons in the excited states, while simultaneously monitoring the transient signatures of the charge character of the excitons in the molecular valence states. We showed that the optical excitation of C_{60} thin films results in the direct formation of excitons with dominant CT character for all molecular coverages between 2 and 20 ML. These CT excitons (CT_2) subsequently decay stepwise into energetically lower CT excitons (CT_1) on sub-100 fs time scales for all coverages before transforming into Frenkel-like excitons. The depopulation time of the CT_1 excitons increases with increasing coverage and saturates at $\tau_{CT1} \approx 3.5$ ps for molecular coverages above 15 ML. Moreover, we did not observe any modification of the exciton population dynamics when changing the light polarization of the optical excitation from p- to s-polarization. This change only results in a reduced number of optically excited excitons for s-polarized light as compared to p-polarized light and hence in a reduction of the optical excitation efficiency of CT excitons in C_{60} films.

In this way, our comprehensive study of the exciton dynamics of fullerene thin films provides a clear view onto transient population decay and the charge character of excitons in molecular thin films. In particular, we demonstrate the crucial role of CT excitons even for the excited-state dynamics of homomolecular fullerene materials and thin films.

■ ASSOCIATED CONTENT

Supporting Information

The Supporting Information is available free of charge at https://pubs.acs.org/doi/10.1021/acs.jpcc.0c08011.

Information to background-corrected raw data of our time- and momentum-resolved photoemission experiment for different molecular coverages as well as all details about the spectral analysis of the excited state and valence band range; along with all information and fitting functions used for the analysis of the population and depopulation time scales of the excited states as well as for the analysis of the time scales of the transient broadening curves; Figure S1, schematic description of data analysis; Figure S2, acquired data for relevant time delays; details on the data acquisition and analysis; and additional references (PDF)

■ AUTHOR INFORMATION

Corresponding Authors

Sebastian Emmerich − *University of Kaiserslautern and Research Center OPTIMAS, Kaiserslautern 67663, Germany; Graduate School of Excellence Materials Science in Mainz (MAINZ), Kaiserslautern 67663, Germany;* orcid.org/0000-0002-7341-7136; Email: emmerich@physik.uni-kl.de

Benjamin Stadtmüller − *University of Kaiserslautern and Research Center OPTIMAS, Kaiserslautern 67663, Germany; Graduate School of Excellence Materials Science in Mainz (MAINZ), Kaiserslautern 67663, Germany;* orcid.org/0000-0001-8439-434X; Email: bstadtmueller@physik.uni-kl.de

Authors

Sebastian Hedwig − *University of Kaiserslautern and Research Center OPTIMAS, Kaiserslautern 67663, Germany*

Benito Arnoldi − *University of Kaiserslautern and Research Center OPTIMAS, Kaiserslautern 67663, Germany*

Johannes Stöckl − *University of Kaiserslautern and Research Center OPTIMAS, Kaiserslautern 67663, Germany*

Florian Haag − *University of Kaiserslautern and Research Center OPTIMAS, Kaiserslautern 67663, Germany; Graduate School of Excellence Materials Science in Mainz (MAINZ), Kaiserslautern 67663, Germany*

Ralf Hemm − *University of Kaiserslautern and Research Center OPTIMAS, Kaiserslautern 67663, Germany*

Mirko Cinchetti − *Experimentelle Physik VI, Technische Universität Dortmund, Dortmund 44221, Germany;* orcid.org/0000-0003-0735-8921

Stefan Mathias − *I. Physikalisches Institut and International Center for Advanced Studies of Energy Conversion (ICASEC), Georg-August-Universität Göttingen, Göttingen 37077, Germany*

Martin Aeschlimann − *University of Kaiserslautern and Research Center OPTIMAS, Kaiserslautern 67663, Germany*

Complete contact information is available at: https://pubs.acs.org/10.1021/acs.jpcc.0c08011

Notes

The authors declare no competing financial interest.

[#]Present Address: (S.E.) Division Mathematics for Vehicle Engineering MF, Fraunhofer Institute for Industrial Mathematics ITWM, Fraunhofer-Platz 1, 67663 Kaiserslautern, Germany.

■ ACKNOWLEDGMENTS

The research leading to these results was funded by the Deutsche Forschungsgemeinschaft (DFG, German Research Foundation) - TRR 173-268565370, project B05. S.E., F.H., and B.S. acknowledge financial support from the Graduate School of Excellence Mainz (Excellence initiative DFG/GSC 266). S.M. acknowledges funding by the Deutsche Forschungsgemeinschaft (DFG, German Research Foundation) - 217133147/SFB 1073, project B07. This work is supported by the European Research Council (Grant 725767-hyControl).

■ REFERENCES

(1) Henson, Z. B.; Müllen, K.; Bazan, G. C. Design Strategies for Organic Semiconductors Beyond the Molecular Formula. *Nat. Chem.* **2012**, *4*, 699−704.

(2) Hiramoto, M.; Kubo, M.; Shinmura, Y.; Ishiyama, N.; Kaji, T.; Sakai, K.; Ohno, T.; Izaki, M. Bandgap Science for Organic Solar Cells. *Electronics* **2014**, *5*, 351−380.

(3) Schwarze, M.; Tress, W.; Beyer, B.; Gao, F.; Scholz, R.; Poelking, C.; Ortstein, K.; Günther, A. A.; Kasemann, D.; Andrienko, D.; et al. Band Structure Engineering in Organic Semiconductors. *Science* **2016**, *352*, 1446−1450.

(4) Bardeen, C. J. The Structure and Dynamics of Molecular Excitons. *Annu. Rev. Phys. Chem.* **2014**, *65*, 127−148.

(5) Kazaoui, S.; Minami, N.; Tanabe, Y.; Byrne, H. J.; Eilmes, A.; Petelenz, P. Comprehensive Analysis of Intermolecular Charge-Transfer Excited States in C_{60} and C_{70} Films. *Phys. Rev. B: Condens. Matter Mater. Phys.* **1998**, *58*, 7689−7700.

(6) Hahn, T.; Tscheuschner, S.; Saller, C.; Strohriegl, P.; Boregowda, P.; Mukhopadhyay, T.; Patil, S.; Neher, D.; Bässler, H.; Köhler, A. Role

of Intrinsic Photogeneration in Single Layer and Bilayer Solar Cells with C_{60} and PCBM. *J. Phys. Chem. C* **2016**, *120*, 25083−25091.
(7) Causa, M.; Ramirez, I.; Martinez Hardigree, J. F.; Riede, M.; Banerji. Femtosecond Dynamics of Photoexcited C_{60} Films. *J. Phys. Chem. Lett.* **2018**, *9*, 1885−1892.
(8) Zhu, X. Y.; Yang, Q.; Muntwilder, M. Charge-Transfer Excitons at Organic Semiconductor Surfaces and Interfaces. *Acc. Chem. Res.* **2009**, *42*, 1779−1787.
(9) Chan, W. L.; Ligges, M.; Jailaubekov, A.; Kaake, L.; Miaja-Avila, L.; Zhu, X. Y. Observing the Multiexciton State in Singlet Fission and Ensuing Ultrafast Multielectron Transfer. *Science* **2011**, *334*, 1541−1545.
(10) Jailaubekov, A. E.; Willard, A. P.; Tritsch, J. R.; Chan, W. L.; Sai, N.; Gearba, R.; Kaake, L. G.; Williams, K. J.; Leung, K.; Rossky, P. J.; et al. Hot Charge-Transfer Excitons Set the Time Limit for Charge Separation at Donor/Acceptor Interfaces in Organic Photovoltaics. *Nat. Mater.* **2013**, *12*, 66−73.
(11) Bernardo, B.; Cheyns, D.; Verreet, B.; Schaller, R. D.; Rand, B. P.; Giebink, N. C. Delocalization and Dielectric Screening of Charge Transfer States in Organic Photovoltaic Cells. *Nat. Commun.* **2014**, *5*, 3245.
(12) Vandewal, K.; Albrecht, S.; Hoke, E. T.; Graham, K. R.; Widmer, J.; Douglas, J. D.; Schubert, M.; Mateker, W. R.; Bloking, J. T.; Burkhard, G. F.; et al. Efficient Charge Generation by Relaxed Charge-Transfer States at Organic Interfaces. *Nat. Mater.* **2014**, *13*, 63−68.
(13) Abramavicius, V.; Pranculis, V.; Melianas, A.; Inganäs, O.; Gulbinas, V.; Abramavicius, D. Role of Coherence and Delocalization in Photo-Induced Electron Transfer at Organic Interfaces. *Sci. Rep.* **2016**, *6*, 32914.
(14) Yan, M.; Rothberg, L. J.; Kwock, E. W.; Miller, T. M. Interchain Excitations in Conjugated Polymers. *Phys. Rev. Lett.* **1995**, *75*, 1992−1995.
(15) Guo, Z.; Lee, D.; Schaller, R. D.; Zuo, X.; Lee, B.; Luo, T.; Gao, H.; Huang, L. Relationship Between Interchain Interaction, Exciton Delocalization, and Charge Separation in Low-Bandgap Copolymer Blends. *J. Am. Chem. Soc.* **2014**, *136*, 10024−10032.
(16) Matheson, A. B.; Ruseckas, A.; Pearson, S. J.; Samuel, I. D. Hole Delocalization as a Driving Force for Charge Pair Dissociation in Organic Photovoltaics. *Mater. Horiz.* **2019**, *6*, 1050−1056.
(17) Stadtmüller, B.; Emmerich, S.; Jungkenn, D.; Haag, N.; Rollinger, M.; Eich, S.; Maniraj, M.; Aeschlimann, M.; Cinchetti, M.; Mathias, S. Strong Modification of the Transport Level Alignment in Organic Materials After Optical Excitation. *Nat. Commun.* **2019**, *10*, 1470.
(18) Rohwer, T.; Hellmann, S.; Wiesenmayer, M.; Sohrt, C.; Stange, A.; Slomski, B.; Carr, A.; Liu, Y.; Miaja-Avila, L. M.; Rohwer, T.; Hellmann, S.; Wiesenmayer, M.; Sohrt, C.; Stange, A.; Slomski, B.; Kalläne, M.; et al. Collapse of Long-Range Charge Order Tracked by Time-Resolved Photoemission at High Momenta. *Nature* **2011**, *471*, 490−493.
(19) Miaja-Avila, L.; Lei, C.; Aeschlimann, M.; Gland, J. L.; Murnane, M. M.; Kapteyn, H. C.; Saathoff, G. Laser-Assisted Photoelectric Effect from Surfaces. *Phys. Rev. Lett.* **2006**, *97*, 113604.
(20) Keunecke, M.; Möller, C.; Schmitt, D.; Nolte, H.; Jansen, G. S. M.; Reutzel, M.; Gutberlet, M.; Halasi, G.; Steil, D.; Steil, S.; et al. Time-Resolved Momentum Microscopy with a 1 MHz High-Harmonic Extreme Ultraviolet Beamline. *Rev. Sci. Instrum.* **2020**, *91*, 063905.
(21) Carley, R.; Döbrich, K.; Frietsch, B.; Gahl, C.; Teichmann, M.; Schwarzkopf, O.; Wernet, P.; Weinelt, M. Femtosecond Laser Excitation Drives Ferromagnetic Gadolinium Out of Magnetic Equilibrium. *Phys. Rev. Lett.* **2012**, *109*, 057401.
(22) Weaver, J. H.; Martins, J. L.; Komeda, T.; Chen, Y.; Ohno, T. R.; Kroll, G. H.; Troullier, N.; Haufler, R. E.; Smalley, R. E. Electronic Structure of Solid C_{60}: Experiment and Theory. *Phys. Rev. Lett.* **1991**, *66*, 1741−1744.
(23) Dresselhaus, M. S.; Dresselhaus, G.; Eklund, P. C. *Science of Fullerenes and Carbon Nanotubes*; Academic Press: Orlando, FL, 1996.
(24) Li, H. I.; Pussi, K.; Hanna, K. J.; Wang, L.-L.; Johnson, D. D.; Cheng, H.-P.; Shin, H.; Curtarolo, S.; Moritz, W.; Smerdon, J. A.; et al. Surface Geometry of C_{60} on Ag(111). *Phys. Rev. Lett.* **2009**, *103*, 056101.
(25) Popmintchev, T.; Chen, M.-C.; Arpin, P.; Murnane, M. M.; Kapteyn, H. C. The Attosecond Nonlinear Optics of Bright Coherent X-Ray Generation. *Nat. Photonics* **2010**, *4*, 822−832.
(26) Mathias, S.; Miaja-Avila, L.; Murnane, M. M.; Kapteyn, H. C.; Aeschlimann, M.; Bauer, M. Angle-Resolved Photoemission Spectroscopy with a Femtosecond High Harmonic Light Source Using a Two-Dimensional Imaging Electron Analyzer. *Rev. Sci. Instrum.* **2007**, *78*, 083105.
(27) Eich, S.; Stange, A.; Carr, A.; Urbancic, J.; Popmintchev, T.; Wiesenmayer, M.; Jansen, K.; Ruffing, A.; Jakobs, S.; Rohwer, T.; et al. Time- and Angle-Resolved Photoemission Spectroscopy with Optimized High-Harmonic Pulses Using Frequency-Doubled Ti:Sapphire Lasers. *J. Electron Spectrosc. Relat. Phenom.* **2014**, *195*, 231−236.
(28) Oloff, L.-P.; Oura, M.; Rossnagel, K.; Chainani, A.; Matsunami, M.; Eguchi, R.; Kiss, T.; Nakatani, Y.; Yamaguchi, T.; Miyawaki, J.; et al. Time-Resolved HAXPES at SACLA: Probe and Pump Pulse-Induced Space-Charge Effects. *New J. Phys.* **2014**, *16*, 123045.
(29) Lopinski, G. P.; Fox, J. R.; Lannin, J. S. Electronic and Vibrational Properties of Laser Modified C_{60}. *Chem. Phys. Lett.* **1995**, *239*, 107−111.
(30) Link, S.; Dürr, H. A.; Eberhardt, W. Femtosecond Spectroscopy. *J. Phys.: Condens. Matter* **2001**, *13*, 7873−7884.
(31) Jacquemin, R.; Kraus, S.; Eberhardt, W. Direct Observation of the Dynamics of Excited Electronic States in Solids: F-sec Time Resolved Photoemission of C_{60}. *Solid State Commun.* **1998**, *105*, 449−453.
(32) Rosenfeldt, A. C.; Göhler, B.; Zacharias, H. Time-Resolved Photoelectron Spectroscopy of Low-Energy Excitations of 4×4 C_{60}/Cu(111). *J. Chem. Phys.* **2010**, *133*, 234704.
(33) Dutton, G.; Quinn, D. P.; Lindstrom, C. D.; Zhu, X. Y. Exciton Dynamics at Molecule-Metal Interfaces: C_{60}/Au(111). *Phys. Rev. B: Condens. Matter Mater. Phys.* **2005**, *72*, 045441.
(34) Dutton, G.; Zhu, X. Y. Distance-Dependent Electronic Coupling at Molecule-Metal Interfaces: C_{60}/Cu(111). *J. Phys. Chem. B* **2004**, *108*, 7788−7793.
(35) Zhu, X. Y. Electronic Structure and Electron Dynamics at Molecule-Metal Interfaces: Implications for Molecule-Based Electronics. *Surf. Sci. Rep.* **2004**, *56*, 1−83.
(36) Shibuta, M.; Yamagiwa, K.; Eguchi, T.; Nakajima, A. Imaging and Spectromicroscopy of Photocarrier Electron Dynamics in C_{60} Fullerene Thin Films. *Appl. Phys. Lett.* **2016**, *109*, 203111.
(37) Latzke, D. W.; Ojeda-Aristizabal, C.; Griffin, S. M.; Denlinger, J. D.; Neaton, J. B.; Zettl, A.; Lanzara, A. Observation of Highly Dispersive Bands in Pure Thin Film C_{60}. *Phys. Rev. B: Condens. Matter Mater. Phys.* **2019**, *99*, 045425.
(38) Haag, N.; Lüftner, D.; Haag, F.; Seidel, J.; Kelly, L.; Zamborlini, G.; Jugovac, M.; Feyer, V.; Aeschlimann, M.; Puschnig, P.; et al. Signatures of an Atomic Crystal in the Band Structure of aC_{60} Thin Film. *Phys. Rev. B: Condens. Matter Mater. Phys.* **2020**, *101*, 165422.
(39) Dutton, G.; Zhu, X. Y. Unoccupied States in C_{60} Thin Films Probed by Two-Photon Photoemission. *J. Phys. Chem. B* **2002**, *106*, 5975−5981.
(40) Varene, E.; Bogner, L.; Bronner, C.; Tegeder, P. Ultrafast Exciton Population, Relaxation, and Decay Dynamics in Thin Oligothiophene Films. *Phys. Rev. Lett.* **2012**, *109*, 207601.
(41) Yagi, H.; Nakajima, K.; Koswattage, K. R.; Nakagawa, K.; Huang, C.; Prodhan, M. S.; Kafle, B. P.; Katayanagi, H.; Mitsuke, K. Photoabsorption Cross Section of C_{60} Thin Films From the Visible to Vacuum Ultraviolet. *Carbon* **2009**, *47*, 1152−1157.

https://dx.doi.org/10.1021/acs.jpcc.0c08011
J. Phys. Chem. C 2020, 124, 23579−23587